Synthesis, crystal structures and properties of lead phosphite compounds

Jun-Ling Song, Chun-Li Hu, Xiang Xu, Fang Kong, Jiang-Gao Mao

www.elsevier.com/locate/yjssc

PII: S0022-4596(15)30134-1
DOI: http://dx.doi.org/10.1016/j.jssc.2015.08.031
Reference: YJSSC19055

To appear in: *Journal of Solid State Chemistry*

Received date: 15 June 2015
Revised date: 12 August 2015
Accepted date: 23 August 2015

Cite this article as: Jun-Ling Song, Chun-Li Hu, Xiang Xu, Fang Kong an Jiang-Gao Mao, Synthesis, crystal structures and properties of lead phosphit compounds, *Journal of Solid State Chemistry* http://dx.doi.org/10.1016/j.jssc.2015.08.031

Synthesis, crystal structures and properties of lead phosphite compounds

Jun-Ling Song, Chun-Li Hu, Xiang Xu, Fang Kong and Jiang-Gao Mao**

State Key Laboratory of Structural Chemistry, Fujian Institute of Research on the Structure of Matter, Chinese Academy of Sciences, Fuzhou 350002, People's Republic of China

Corresponding author. Tel.: +86-59183736672; fax: +86-59183714946. E-mail address: s070054@e.ntu.edu.sg, mjg@fjirsm.ac.cn

Highlights

- A new lead phosphite, $Pb_2(HPO_3)_2$ is reported.
- $Pb_2(HPO_3)_2$ features a unique 3D framework structure.
- NLO property of $Pb_2(HPO_3)(NO_3)_2$ is investigated.
- $Pb_2(HPO_3)(NO_3)_2$ produces a moderate SHG response of ~1.8×KDP (KH_2PO_4).

Abstract

Here, we report the preparation and characterization of two lead(II) phosphites, namely, $Pb_2(HPO_3)_2$ and $Pb_2(HPO_3)(NO_3)_2$ through hydrothermal reaction or simple solution synthesis, respectively. A new lead phosphite, namely, $Pb_2(HPO_3)_2$, crystallizes in the noncentrosymmetric space group $Cmc2_1$ (no. 36), which features 3D framework formed by the interconnection of 2D layer of lead(II) phosphites and 1D chain of $[Pb(HPO_3)_5]_\infty$. The nonlinear optical properties of $Pb_2(HPO_3)(NO_3)_2$ have been studied for the first time. The synergistic effect of the stereo-active lone-pairs on Pb^{2+} cations and π-conjugated NO_3 units in $Pb_2(HPO_3)(NO_3)_2$ produces a moderate second harmonic generation (SHG) response of

~1.8×KDP (KH_2PO_4), which is phase matchable (type I). IR, UV-vis spectra and thermogravimetric analysis (TGA) for the two compounds were also measured.

Keywords

Crystal structure, π-conjugated unit, lead phosphites, NLO property, synergistic effect.

1. Introduction

During the past several decades, numerous investigations have been carried out on new second-order nonlinear optical (NLO) materials due to their applications in the wavelength conversions, high density optical storage and signal communication [1-6]. Among these reported NLO materials, metal phosphates have attracted increasing research interest because of their unique architectures and their wide applications in catalysis, gas storage and nonlinear optics, etc [7-11]. As a polarizable building unit, the regular tetrahedra PO_4^{3-} unit with point group (symmetry T_d) might result in materials with good NLO property. Specifically, KH_2PO_4 (KDP) and $KTiOPO_4$ (KTP) have been extensively used for visible and UV second harmonic generation [7], however, metal phosphate species still need to be expanded in order to further discover new materials with excellent NLO performance. Thus, it is still urgent, and is a challenge task, to search this family of compounds with abundant structures and good properties. The phosphite group $(HPO_3)^{2-}$ is closely related to the phosphate group, moreover, the irregular $(HPO_3)^{2-}$ tetrahedra (symmetry C_{3v}) which replace the PO_4^{3-} tetrahedra may lead to more novel compounds with noncentrosymmetric (NCS) structure. Numerous alkaline, alkaline earth and transition metal phosphites with various structure types have been synthesized and characterized [12-16]. Generally, in these metal phosphites, $[HPO_3]^{2-}$ anions link the cations into low-dimensional coordination polymers that are connected into higher dimension through hydrogen bonds, which are similar to the chemical bonds involved in KDP. However, to our best knowledge, metal phosphites with NLO properties are still rare, two compounds, namely, $SnHPO_3$ [12] and $RbIn(HPO_3)_2$ [13] exhibit relatively weak SHG responses since the lone pair of the P^{3+} cation is not SHG active. To date, significant efforts have also been made to search compounds with excellent SHG properties and it has been demonstrated that employing

asymmetric building units or polarizable building units offers an excellent strategy for synthesizing new NLO materials. The above-mentioned units mainly consist of d^0 early transition-metal cations with second order Jahn-Teller effect, metal ions with stereo-chemically active lone pair, such as $5s^2$ Sn^{2+}, $6s^2$ Tl^+, Pb^{2+} and Bi^{3+} ions or π-conjugated system such as borate, nitrate and carbonate [3-6]. Introducing the lone electron-pair or planar units into the same system might lead to the large induced polarizability which could enhance the NLO property of materials according to the previous works [3-6]. Furthermore, compounds based on cations containing lone-pair electrons and π-conjugated planar triangular units have been shown good NLO performance such as $Pb_2B_5O_9I$ [17], $CsPbCO_3F$ [18] and $Bi_2O_2[NO_3(OH)]$ [19] with large SHG responses of about 13.5, 13.4 and 6.0 times that of KDP, respectively. Recently, we also found that combination of the stereo-active lone pairs on Pb^{2+} cations and two type of π-conjugated units could result in new second-order NLO compounds with high SHG coefficient [20]. Therefore, it should be a positive effect to introduce cation with ns^2 lone pairs into metalphosphite systems. Thus, in this work, our research interests focus on the effects of the Pb^{2+} cations with lone pairs and NO_3 π-conjugated unit on the structures formation and property of the metal phosphite systems and we expect that synergistic effect of the stereo active lone pairs on Pb^{2+} polyhedra and the planar triangle group may produce new NLO materials. Our research efforts led to two 3D frameworks lead phosphites, namely, $Pb_2(HPO_3)_2$ and $Pb_2(HPO_3)(NO_3)_2$, where the structure of $Pb_2(HPO_3)(NO_3)_2$ was reported previously by Ouarsal et al. [21] While, the NLO property of this compound was not studied in the literature. Herein, we report the crystal structure of $Pb_2(HPO_3)_2$, syntheses of two compounds, their optical properties, thermal stability and NLO properties.

2. Experimental section

2.1. Materials and Methods. $Pb(NO_3)_2$, $PbCO_3$ and H_3PO_3 aqueous solution (50%) were purchased from Shanghai Reagent Factory (AR, 99.0%) and used without further purification. IR spectra were recorded on a Magna 750 Fourier transform infrared (FT-IR) spectrometer as KBr pellets in the range of

4000-450 cm^{-1} with a resolution of 2 cm^{-1} at room temperature. Optical diffuse reflectance and UV spectra were measured at room temperature with a Perkin-Elmer Lambda 900 UV-Vis-NIR spectrophotometer and a $BaSO_4$ plate was used as a standard (100% reflectance). The absorption spectrum was calculated from reflectance spectra using the Kubelka-Munk function: $\alpha/S = (1-R)^2/2R$, where α is the absorption coefficient, S is the scattering coefficient (which is practically wavelength independent when the particle size is larger than 5 μm), and R is the reflectance [22]. X-ray powder diffraction (XRD) patterns were collected on a Rigaku MiniFlex II diffractometer using Cu-$K\alpha$ radiation in the angular range of 2θ = 5-80 ° with a step size of 0.1°. Thermogravimetric analyses (TGA) and differential scanning calorimetry (DSC) analyses were carried out with a NETZCH STA449C unit at a heating rate of 15 ℃ min^{-1} under N_2 and air atmosphere. The measurement of the powder frequency-doubling effects was carried out on the sieved samples by means of the modified method of Kurtz and Perry [23]. The 1064 nm radiations generated by a Q-switched Nd:YAG solid-state laser were used as the fundamental frequency light, respectively. The crystals of $Pb_2(HPO_3)(NO_3)_2$ were ground and sieved into several distinct particle size ranges (0-25, 25-45, 45-53, 53-75, 75-105, 105-150, 150-210 and 210−270 μm). Sieved KH_2PO_4 (KDP) powders (150-210 μm) as standard was used as a reference material to survey the SHG effect. X-ray diffraction data collection for $Pb_2(HPO_3)_2$ was performed on a Rigaku Mercury CCD diffractometer with Mo-Kα radiation (λ = 0.71073 Å) at 293(2) K. The data sets were corrected for Lorentz and polarization factors as well as absorption by the multi-scan method [24]. The structure was solved by the direct method and refined by full-matrix least-squares fitting on F^2 by SHELX-97 [25]. All non-hydrogen atoms were refined with anisotropic thermal parameters. According to the charge balance and bond valence calculations, all the H atoms in $Pb_2(HPO_3)_2$ were needed and assigned to P-H bonds, but they were not refined due to the difficulty in the determination of their precise locations. Pb(2), Pb(3), P(1), P(3), O (2) and O(7) lie in a crystallographic mirror plane, hence, their occupancy are 0.5. The structure was also checked for possible missing symmetry with PLATON. Crystallographic data and structural refinements are summarized in Table 1. Atomic coordinates ($\times 10^4$)

and equivalent isotropic displacement parameters, important bond distances and angles are listed in Table S1 and S2, respectively. Further details of the crystal structure studies can be obtained from the FIZ Karlsruhe, 76344 Eggenstein-Leopoldshafen, Germany (Fax: (49)7247808666; E-mail: crysdata@fiz-karlsruhe.de), on quoting the depository numbers CSD 429745.

2.2. Synthesis

Synthesis of $Pb_2(HPO_3)_2$ (1). $Pb_2(HPO_3)_2$ was synthesized hydrothermally in a 20-mL Teflon-lined autoclave by heating a mixture of $PbCO_3$ (0.668 g, 2.5 mmol), H_3PO_3 solution (1.0 mL) and H_2O (10.0 mL) at 210 ^oC for 4 days. The initial and final pH values are 1.5 and 1.0, respectively. The colorless prism-shaped $Pb_2(HPO_3)_2$ crystals were obtained in a yield of ca. 65% based on Pb. The experimental X-ray powder diffraction pattern is in agreement with the one simulated from the single-crystal crystallographic data (See Supplementary Fig. S1). IR data (KBr cm^{-1}): 3791 (w), 3677 (w), 3550 (w), 2476 (w), 2570 (w), 2334 (s), 2050 (w), 2008 (w), 1658 (w), 1355 (w), 1062 (vs), 593 (m), 470 (m).

Synthesis of $Pb_2(HPO_3)(NO_3)_2$ (2). $Pb_2(HPO_3)(NO_3)_2$ was synthesized according to a reported method with slightly modification [21]. $Pb(NO_3)_2$ (0.497 g, 1.5 mmol) and H_3PO_3 solution (1.0 mL) were mixed in distilled water (5 mL), and the mixture was stirred at 80 ^oC for 3 hrs. The resultant solution was filtered and allowed to evaporate slowly until many colorless needle crystals of $Pb_2(HPO_3)(NO_3)_2$ were obtained in a yield of ca. 50 %. The experimental X-ray powder diffraction pattern is in agreement with the one simulated from the single-crystal crystallographic data (Fig. S1). IR data (KBr cm^{-1}): 3570 (w), 3460 (w), 2410 (w), 2329 (m), 2400 (w), 2065 (w), 1766 (m), 1587 (m), 1587 (m), 1374 (vs), 1062 (vs), 688 (m) 598 (vs), 470 (m).

3. Results and Discussion

3.1. Crystal Structure

$Pb_2(HPO_3)_2$ crystallizes in the polar orthorhombic space group *C*mc2_1 (no. 36) and features a 3D framework formed by the interconnection of 2D layer of lead phosphites and 1D chain of

$[Pb(HPO_3)_5]_\infty$ (Fig. 1). The asymmetric unit of $Pb_2(HPO_3)_2$ includes 13 independent non-H atoms, including three Pb, three P and seven O atoms. Pb(2), Pb(3), P(1) and P(3) lie in a crystallographic mirror plane. Pb(1) is six coordinated by six oxygens from five HPO_3 anions in a distorted pentagonal pyramid geometry, Pb(2) is five coordinated by five oxygens from five HPO_3 anions in a tetragonal pyramid geometry, while Pb(3) is seven coordinated by seven oxygens from six HPO_3 anions in a distorted heptagonal pyramid geometry. The Pb–O bonds of three PbO_x (x = 5, 6 or 7) polyhedra are located at the same side of the Pb atom, thus, all of the Pb^{2+} ions show stereochemically active lone pairs. The Pb−O distances range from 2.333(10) to 2.91(2) Å, comparable to those reported for other lead(II) phosphites [21]. The bond valence sums (BVSs) of the Pb^{2+} cation obtained by the bond valence calculations are 1.66, 1.68 and 1.50, respectively, which are slightly smaller than the ideal oxidation state of +2 [26-28]. The deviation of the Pb atoms from the expected BVS value of +2 indicates that there are other weak Pb−O bonds (Pb−O bond length from 2.9 to 3.1 Å). Each P atom bonds to three oxygen atoms and one hydrogen atom with P−O bond distances ranging from 1.49(2) to 1.532(15) (Table S2) and adopt pseudo-tetrahedral coordination geometry. In addition, the IR absorption band at 2334 cm^{-1} confirms the existence of P-H bonds in HPO_3^{2-} anions (Fig. S2). The BVSs of the PH^{4+} cation obtained according to the bond valence calculations are 3.78, 3.81 and 3.71, respectively, which are in good agreement with the oxidation state of the PH^{4+} group [29]. Three phosphite anions adopts different coordination modes as shown in Scheme 1. $HP(1)O_3$ anion shows a μ_5-$\eta^2\eta^2\eta^3$-coordination mode (5.223) that bridges and chelates 5 Pb atoms (Scheme 1a), $HP(2)O_3$ anion displays 5.122 coordination mode that bridges 5 Pb atoms (Scheme 1b), and $HP(3)O_3$ anion adopts 6.133 coordination mode that bridges and chelates 6 Pb atoms (Scheme 1c). Pb(1) and Pb(3) are linked by O atoms from phosphite anions to form a Pb binuclear cluster via corner- and edge-sharing oxygen atoms. Each binuclear cluster further connects each other by HPO_3 anion into a 2D layer of lead phosphites along the *c* axis (Fig. 1a). While, the interconnection of $Pb(2)O_5$ polyhedra via edge-sharing oxygen atoms results in a 1D $[Pb(HPO_3)_5]_\infty$ chain along the *c* axis (Fig. 1b). Such 1D $[Pb(HPO_3)_5]_\infty$

chain further bridges the above 2D layer by corner-sharing oxygen atom to yield a 3D framework in the *ab* plane (Fig. 1c). Even though both compound $Pb_2(HPO_3)_2$ (**1**) and $Pb_2(HPO_3)(NO_3)_2$ (**2**) possess 3D open-frameworks structure, their topologies are different. As mentioned above, in compound **1**, the lead metal centers are joined into three dimensional networks by the oxygen atoms from HPO_3^{2-} anion via corner-sharing and edge-sharing. While, in compound **2**, $Pb(1)O_6$ and $Pb(2)O_{10}$ are connected by HPO_3 tetrahedron respectively, leading to two kinds of 2D layer, further, this 2D layer are joined together to form three-dimensional network. Moreover, the fusion of the $Pb(1)O_6$ and $Pb(2)O_{10}$ building blocks produces 10 and 6-membered channels along *a*-axis (Fig. S3) Two NO_3 units are located at the above 10-membered channels. HPO_3^{2-} anion in compound **2** is pentadentate, adopting 5.122 coordination mode, which is the same as $HP(2)O_3$ anion in $Pb_2(HPO_3)_2$ compounds. In addition, one NO_3 chelates three Pb(2) atoms bidentately and other NO_3 chelates one Pb(2) atom bidentately and also bridges with three Pb(1) atoms. Thereby, the introduction of planar triangle NO_3^- anion leads to the forming of a novel 3D frameworks with enormous open channels in compound **2** and might affect its relevant properties.

3.2. Optical properties

Optical diffuse-reflectance spectra indicate that $Pb_2(HPO_3)_2$ and $Pb_2(HPO_3)(NO_3)_2$ are wide band-gap semiconductors with optical band gaps of 3.97 and 3.81 eV, respectively (Fig. 2). UV-vis-NIR absorption spectra of $Pb_2(HPO_3)_2$ and $Pb_2(HPO_3)(NO_3)_2$ show one strong absorption in the region of 200 to 400 nm, which mainly originates from the charge transfer transition from O to Pb (Fig. S4). The IR spectra of two compounds are similar as shown in Fig. S2. The characteristic band at 2334 cm^{-1} and 2329 cm^{-1} for $Pb_2(HPO_3)_2$ and $Pb_2(HPO_3)(NO_3)_2$, respectively, is attributed to the stretching vibration of the P-H bonds. The strong absorption peak at 1374 cm^{-1} is due to the asymmetric stretch (ν_{as}) of NO_3, and band at 825 cm^{-1} may be assigned as the NO_3 in-plane deformation (δ), which confirm the presence of NO_3^- group in compound $Pb_2(HPO_3)(NO_3)_2$. The strong band at 1057 cm^{-1} for $Pb_2(HPO_3)_2$ or 1062 cm^{-1} for $Pb_2(HPO_3)(NO_3)_2$ corresponds to the stretching vibrations (ν_{as}) of PO_3 group. The bands at 1722 and 1587 cm^{-1} for compound $Pb_2(HPO_3)(NO_3)_2$ can be attributed to the stretching vibrations of the

non-coordinating oxygen atoms of the nitrate group. The bands in the range of 450-600 cm^{-1} for $Pb_2(HPO_3)_2$ and $Pb_2(HPO_3)(NO_3)_2$ are ascribed to the banding vibrations of PO_3 groups.

3.3. TGA Studies. Fig. 3 shows thermogravimetric analysis of two compounds under nitrogen gas. Compound $Pb_2(HPO_3)_2$ exhibits one slight weight loss in the range of 100-380 ^oC, corresponding to the removal of water molecule.No weight loss was observed between the temperature range 400-750 °C, while the weight of this compound is slightly increasing during 750 to 850 ^oC, probably due to the partial oxidation of partial oxidation of phosphite to phosphate [13]. After that the compound starts to decompose continuously and the final residuals become amorphous. The TGA curve of $Pb_2(HPO_3)(NO_3)_2$ indicates that it thermally stable up to about 200 ^oC under nitrogen atomsphere. Then it mainly displays two steps of weight loss, the weight loss in the temperature range 200-325 ^oC corresponds to the release of water molecule and NO_3 group. The other weight loss was observed between the temperature range 425-515 °C, corresponding to the further decomposition of nitrate groups. After dehydration and decomposition, no weight lose was observed up to about 1000 ^oC (Fig. 3). The total weight loss of about is 15.86%, which corresponds to the decomposition of water, NO_3 and PO_3 groups. The final residuals are not characterized because of their amorphous nature.

3.4. Theoretical studies

To further investigate the band structure and density of states (DOS) of compound, theoretical calculations based on DFT methods were performed by using the computer code CASTEP. Compound $Pb_2(HPO_3)(NO_3)_2$ containing Pb^{2+}, HPO_3 and NO_3 units was discussed in detail. The band structure calculations indicate that $Pb_2(HPO_3)(NO_3)_2$ is a direct band-gap compound with a band gap of 3.39 eV since both the lowest conduction band and the highest valence band are localized at the X point (Fig. S5). The calculated band gap is smaller than the experimental value (3.81 eV) which is attributed to the underestimation of the band gap by using DFT-GGA method [30]. The total and partial DOS were plotted in Fig. S6. The valence band in the range from -20.0 and -16.0 eV comes from mostly O-2s with a small amount of P-2s2p and N-2p states. The peak localized around −14.0 almost arises from isolated

Pb-5d. The bands near the Fermi level (from -10.0 to 0 eV in the valence band and from 3.0to 7.1 eV in the conduction band) are mainly predominately derived from the O-2s2p, N-2s2p, P-2s2p, Pb-6s6p and H-1s states, indicating the strong covalent interactions of Pb-O, N-O, P-O and H−P bonds in the compound. Both valance band maximum and conduction band minimum are mainly from the electronic states of NO_3 and Pb-O units, thus, NO_3^- unit has a dominant effect on the band gap of the $Pb_2(HPO_3)(NO_3)_2$.

3.5. NLO Properties

Since $Pb_2(HPO_3)_2$ and $Pb_2(HPO_3)(NO_3)_2$ are acentric structurally, their SHG response were investigated on a Q-switched Nd:YAG laser with the sieved crystal samples according to the method provided by Kurtz and Perry [23]. By using commercially available NLO crystal, optical quality KDP, as a reference, $Pb_2(HPO_3)(NO_3)_2$ shows a moderate SHG response of about 1.8× KDP and is also phase-matchable (Fig. 4), whereas $Pb_2(HPO_3)_2$ displays no SHG signals. In order to go deeper into the structures-properties relationship to understand their NLO better, we calculated the dipole moments of NLO-active units in their structure. In $Pb_2(HPO_3)_2$, the contribution for the SHG effect is mainly from the lone pair electrons of the Pb^{2+} cation. Since the lone pair of the P^{3+} cation is inert due to the presence of H-P bonds in the structures, the NLO-active units are mainly arising from the Pb-O polyhedra. Therefore, the local dipole moments of PbO_x polyhedra (x= 5, 6 or 7) in $Pb_2(HPO_3)_2$ unit cell were calculated by using a method reported earlier [31-32]. The results showed that the *x*, and *y*-component of the polarizations within one unit cell for $Pb(1)O_6$, $Pb(2)O_5$ and $Pb(3)O_7$ polyhedra are offset completely, whereas the *z*-components add to produce a small net dipole moment of -0.536 D along the *c* axis. Hence, the dipole moments associated with PbO_x polyhedra have largely been canceled out. As a result no obvious SHG signal was observed in $Pb_2(HPO_3)_2$. Whereas $Pb_2(HPO_3)(NO_3)_2$ contains two different typess of NLO-active groups, π-conjugated NO_3 unit and lead oxygen polyhedra. The contribution from lead oxygen polyhedra was estimated by calculating the local dipole moments, and the result shows that *x*- and *y*-components are almost counterbalanced, while the dipole moment value of *z*-component is 4.335 D

which is still not remarkable. Base on the anionic group theory, the SHG coefficient mainly induced by the π-conjugated planar units in its structure, which is proportional to density of the planar π-conjugated units and the geometric factor (*g*) [33-36]. In this case, together with Pb-O polyhedral NLO-active units, the moderate density (n/V = 0.00988 $Å^{-3}$) of the $[NO_3]^-$ in $Pb_2(HPO_3)(NO_3)_2$ makes the majority contribution to its NLO coefficient [34]. Thus, based on the above discussion and analysis, the synergistic effect of the stereo-active lone-pairs on Pb^{2+} cations and the π-conjugated NO_3 units lead to a moderate SHG response of ~1.8×KDP. The planar triangle NO_3^- anion being introduced into the structure could improve the NLO performance of phosphite materials.

4. Conclusions

In summary, we reported UV-vis-near IR absorption spectroscopy and IR spectroscopy, TGA and NLO property of two lead phosphites. A new lead phosphites, namely, $Pb_2(HPO_3)_2$, was obtained and it crystallizes in the noncentrosymmetric space group *C*mc2_1, which features 3D framework formed by the interconnection of 2D layer of lead(II) phosphites and 1D chains of $[Pb(HPO_3)_5]_\infty$. This study also demonstrates that the introduction of planar triangle NO_3^- anion could lead to different products and also affect the property of the lead-phoshites. Also, the planar triangle NO_3^- unit has a dominant effect on the band gap of the compound and make a greater contribution to NLO coefficient of metal phoshites. We believe that other planar triangle anion such CO_3^{2-} or BO_3^{3-} anions may be introduced into the lead-phosphites system, which might lead to other related lead-phosphites with good NLO performance. In future work, we will devote research to exploit other related systems and will study the synthesis, crystal structures and properties of other related materials.

Acknowledgment. This work was supported by the National Natural Science Foundation of China (Nos.2123006 and 21403232) and the Scientific Research Foundation for the Returned Overseas Chinese Scholars, State Education Ministry (SRF for ROCS, SEM).

References:

1. K. M. Ok, E. O. Chi, P. S. Halasyamani, *Chem. Soc. Rev*., 35(2006), pp.710-717.

2. S. V. Krivovichev, O. Mentré, O. I. Siidra, M. Colmont and S. K. Filatov, *Chem. Rev.*, 113(2013), pp. 6459-6535.

3. R. Mu, Q. Fu, L. Jin, L. Yu, G. Fang, D. Tan and X. Bao, *Angew. Chem., Int. Ed*., 51(2012), pp. 4856-4859.

4. H. Wu, S. Pan, K. R. Poeppelmeier and J. M. Rondinelli, *J. Am. Chem. Soc*., 135(2013), pp. 4215-4218.

5. S. C. Wang, N. Ye, W. Li and D. Zhao, *J. Am. Chem. Soc.*, 132(2010), pp. 8779-8786.

6. H. Huang, J. Yao, Z. Lin, X. Wang, R. He, W. Yao, N. Zhai and C. Chen, *Angew. Chem., Int. Ed.* 50(2011), pp. 9141-9144.

7. T. A. Driscoll, H. J. Hoffman, R. E. Stone, P. E. Perkins, *J. Opt. Soc. Am. B* 3(1986), pp. 683-686.

8. J. Liang, J. Li, J. Yu, P. Chen, F. Sun and R. Xu, *Angew. Chem., Int. Ed*., 45(2006), pp. 2546-2548.

9. T. K.Bera, J. I. Jang, J. B. Ketterson, M. G. Kanatzidis, *J. Am. Chem. Soc*. 131(2009), pp. 75-77.

10. P. Yu, L. M. Wu, L. J. Zhou, L. Chen, *J. Am. Chem. Soc*. 136(2014), pp. 480-487.

11. S. G. Zhao, P. F. Gong, S. Y. Luo, L. Bai, Z. S. Lin, C. M. Ji, T. L. Chen, M. C. Hong, and J. H. Luo *J. Am. Chem. Soc.*, 136(2014), pp. 8560-8563.

12. H.-L. Huang,Y.-C. Lai,Y.-W. Chiang and S.-L.Wang *Inorg. Chem.*, 51(2012), pp. 1986-1988.

13. X.-J. Wang, J.-H. Zhang, J.-L. Song, F. Kong and J.-G. Mao, *CrystEngComm*, 15(2013), pp. 2519-2526. |

14. H. Z. Xing, W. T. Yang, T. Su, Y. Li, J. Xu, T. Nakano, J. H. Yu, R. R. Xu, *Angew. Chem.*

Int. Ed, 49(2010), pp. 2328-2331.

15. M. P. Attfield, R. E. Morris, A. K. Cheetham, *Acta Cryst. C* 50(1994), pp. 981-984.

16. G. B. Johansson, O. Lindqvist, *Acta Cryst. B* 32(1976), pp. 412-414.

17. Y. Z. Huang, L. M. Wu, X. T. Wu, L. H. Li, L. Chen, and Y. F. Zhang, *J. Am. Chem. Soc*., 132(2010), pp. 12788-12789.

18. G. H. Zou, L. Huang, N. Ye, C. S. Lin, W. D. Cheng and H. Huang, *J. Am. Chem. Soc*., 135(2013), pp. 18560-18566.

19. R. H. Cong, T. Yang, F. H. Liao, Y.X. Wang, Z. S. Lin, J. H. Lin, *Mater. Res. Bull*. 47(2012), pp. 2573-2578.

20. J.-L. Song, C.-L. Hu, X. Xu, F. Kong and J.-G. Mao, *Angew. Chem., Int. Ed.,* 54(2015), pp. 3679-3682.

21. R. Ouarsal, M. Lachkar, Michal Dušek, K. Fejfarovãb and B. E. Balic, *Acta Cryst. E* 65 (2009), pp. i35.

22. W. M. Wendlandt and H. G. Hecht, *Reflectance Spectroscopy; Interscience*: New York, 1966.

23. S. K. Kutz, T. T. Perry, *J. Appl. Phys*. 39(1968), pp. 3798.

24. (a) *CrystalClear*, *Version 1.3.5*; Rigaku Corp.: Woodlands, TX, 1999. (b) G. M. Sheldrick, SHELXTL, Crystallographic Software Package, *SHELXTL*, Version 5.1; Bruker-AXS: Madison, WI, 1998. (c) A. L. Spek, *J. Appl. Crystallogr*., 36(2003), pp.7-13.

25. (a) I. D. Brown and D. Altermatt, *Acta Crystallogr. B* 41(1985) pp. 244-247; (b) N. E. Brese and M. O'Keeffe, *Acta Crystallogr. B* 47(1991), pp.192-197.

26. S. S. Huang, H. W. Yu, J. Han, S. L. Pan, Q. Jing, Y. Wang, L. Y. Dong, H. P. Wu, Z. H. Yang, and X. Wang, *Eur. J. Inorg. Chem.* 22(2014), pp. 3467-3473.

27. H. R. Tian, W. H. Wang, Y. E. Gao, T. T. Deng, J. Y. Wang,Y. L. Feng, J. W. Cheng, *Inorg. Chem.* 52(2013), pp. 6242-6244.

28. J. L. Song, C. L. Hu, X. Xu, F. Kong, J.G. Mao, *Inorg. Chem.* 52(2013), pp. 8979-8986.

29. F. Hamchaoui, V. Alonzo, D.Venegas-Yazigi, H. Rebbah, E. Le Fur *J. Solid State Chem*. 198(2013), pp. 295-302.

30. J. P. Perdew, K. Burke, M. Ernzerhof, *Phys. Rev. Lett*. 77(1996), pp. 3865-3868.

31. C.-F. Sun , C.-L. Hu, X. Xu, B.-P. Yang, and J.-G. Mao, *J. Am. Chem. Soc.*, 133(2011), pp. 5561-5572.

32. H. Y. Chang, S. H. Kim, K. M. Ok, P. S. Halasyamani, *Chem. Mater*. 21(2009), pp.1654-1662.

33. C. T. Chen, G. Z. Liu, *Annu. Rev. Mater. Res*. 16(1986), pp. 203-43.

34. G. X. Wang, M. Luo, N. Ye, C. S. Lin and W. D. Cheng, *Inorg. Chem.*, 53(2014), pp. 5222-5228.

35. L. X. Chang, L. Wang, X. Su, S. L. Pan, R. Hailili, H.W. Yu and Z. H. Yang, *Inorg. Chem*., 53(2014), pp. 3320-3325.

36. S. C. Wang, N. Ye, W. Li and D. Zhao, *J. Am. Chem. Soc*., 132(2010), pp. 8779-8786.

Figure and table captions

Scheme 1. Three coordination modes of phosphoric acid.

Table 1. Crystal data and structural refinement for $Pb_2(HPO_3)_2$.

Fig. 1. A lead(II) phosphites layer perpendicular to the *c* axis (a), 1D chains of $[Pb(HPO_3)_5]_\infty$ along the *c*-axis (b), and view of structure of compound $Pb_2(HPO_3)_2$ down the *c* axis (c).

Fig. 2. Optical diffuse reflectance spectra for $Pb_2(HPO_3)_2$ (a) and $Pb_2(HPO_3)(NO_3)_2$ (b) .

Fig. 3. TG and DTA diagrams for $Pb_2(HPO_3)_2$ (a) and $Pb_2(HPO_3)(NO_3)_2$ (b).

Fig. 4 Oscilloscope traces of the SHG signals for the powders (150-210 μm) of KDP and $Pb_2(HPO_3)(NO_3)_2$ (a), and the phase-matching curve for $Pb_2(HPO_3)(NO_3)$ (b).

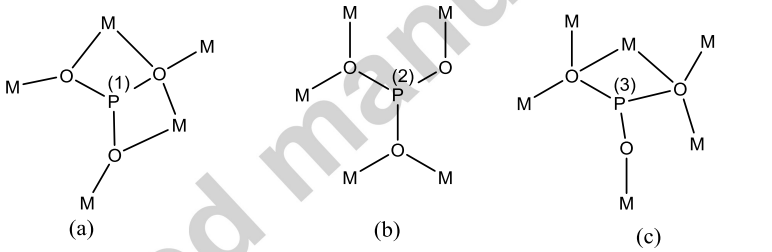

(μ_5-$\eta^2\eta^2\eta^3$) (μ_5-$\eta^1\eta^2\eta^2$) (μ_6-$\eta^1\eta^3\eta^3$)

Scheme 1.

Table 1.

Compound	**1**
Empirical formula	$Pb_2(HPO_3)_2$
Formula weight	574.36
Crystal system	Orthorhombic
Space group	*C*mc2_1
Temperature	293(2) K
Wavelength	0.71073 A
a/Å	11.1374(3)
b/Å	14.3087(3)
c/Å	8.1439(2)
V/Å^3	1297.83(5)
Z	8
D_c/g·cm^{-3}	5.879
μ(Mo Kα)/mm^{-1}	52.282
Completeness to theta = 26.37	99.9 %
Goodness-of-fit on F^2	1.077
Final R indices [I>2sigma(I)][a]	R_1 = 0.0391, wR_2 = 0.0984
R indices (all data)	R_1 = 0.0407, wR_2 = 0.0997
Absolute structure parameter	0.50(3)
Largest diff. peak and hole	4.591 and -3.134 e. Å^{-3}

[a] $R_1 = \Sigma||F_o|-|F_c||/\Sigma|F_o|$, $\omega R_2 = \{\Sigma\omega[(F_o)^2 (F_c)^2]^2/\Sigma\omega[(F_o)^2]^2\}^{1/2}$.

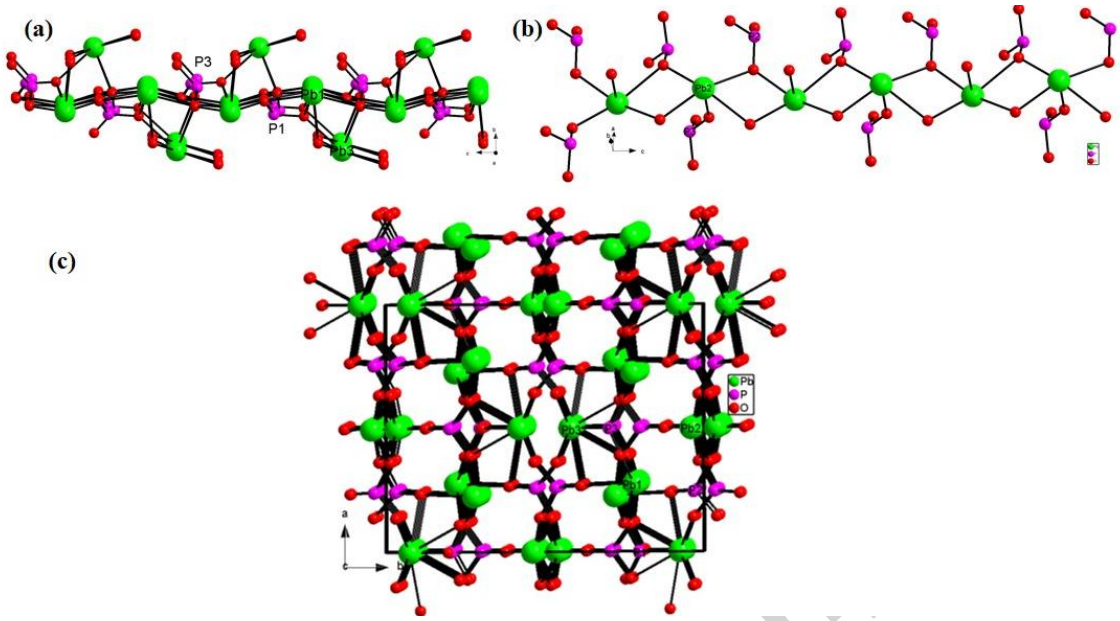
(a)
P3
Pb
P1
Pb3
(b)
Pb2
(c)
Pb
P
O
Pb3
Pb2
P1
a
c
b

Fig. 1.

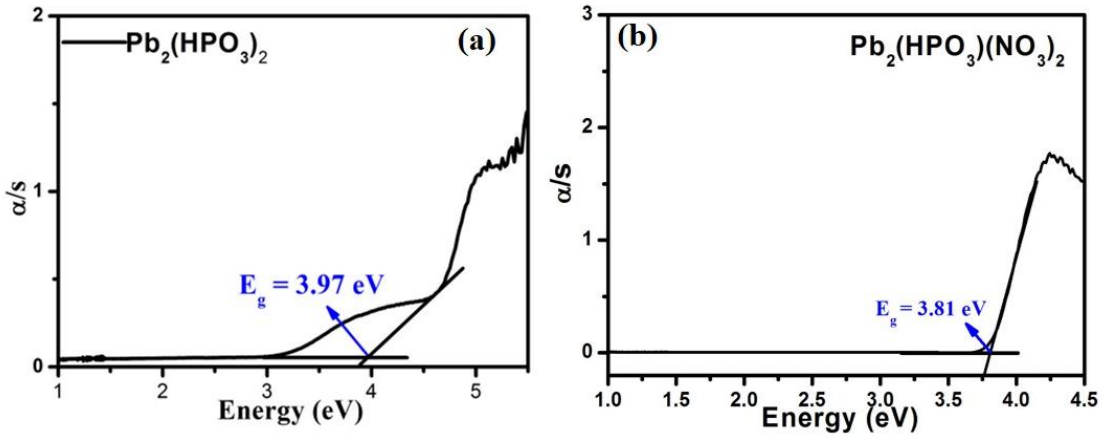
Pb2(HPO3)2
(a)
α/s
Eg = 3.97 eV
Energy (eV)
(b)
Pb2(HPO3)(NO3)2
α/s
Eg = 3.81 eV
Energy (eV)

Fig. 2.

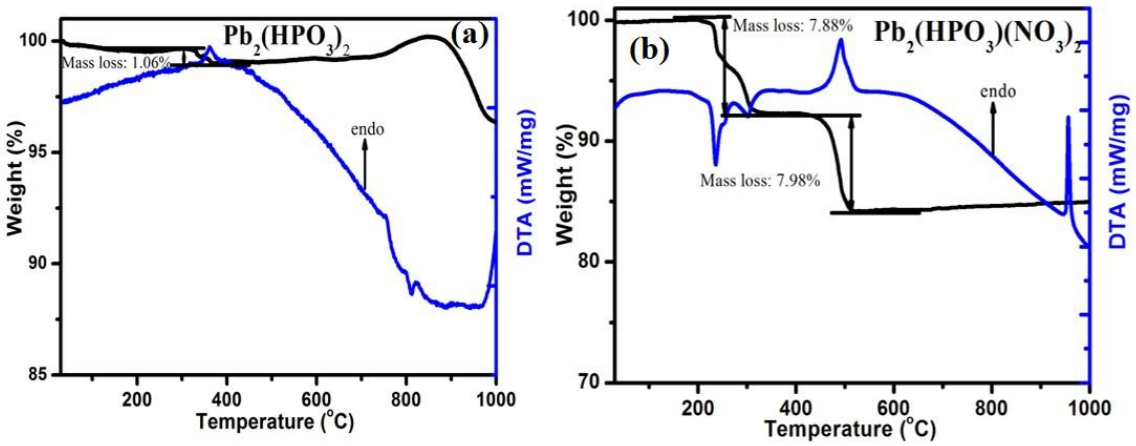
Pb2(HPO3)2
(a)
Mass loss: 1.06%
endo
Weight (%)
DTA (mW/mg)
Temperature (°C)
(b)
Mass loss: 7.88%
Pb2(HPO3)(NO3)2
endo
Mass loss: 7.98%
Weight (%)
DTA (mW/mg)
Temperature (°C)

Fig. 3.

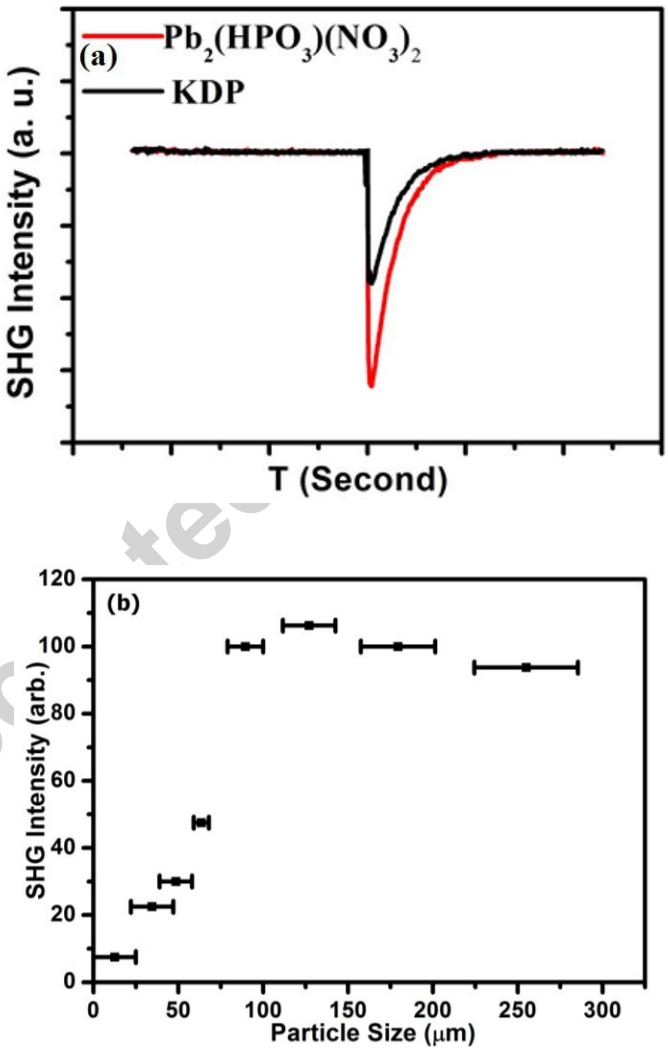
Pb2(HPO3)(NO3)2
(a)
KDP
SHG Intensity (a. u.)
T (Second)
(b)
SHG Intensity (arb.)
Particle Size (μm)

Fig. 4.

Supplementary materials

Synthesis, crystal structures and properties of lead phosphite compounds

Jun-Ling Song, Chun-Li Hu, Xiang Xu, Fang Kong and Jiang-Gao Mao**

State Key Laboratory of Structural Chemistry, Fujian Institute of Research on the Structure of Matter, Chinese Academy of Sciences,

Fuzhou 350002, People's Republic of China

Corresponding author. Tel.: +86-59183736672; fax: +86-59183714946. E-mail address: s070054@e.ntu.edu.sg, mjg@fjirsm.ac.cn

Table S1. Atomic coordinates ($\times 10^4$) and equivalent isotropic displacement parameters ($Å^2 \times 10^3$) for $Pb_2(HPO_3)_2$. U_{eq} is defined as one third of the trace of the orthogonalized U_{ij} tensor.

Table S2. Bond distances (Å) and angles [^{o}] for $Pb_2(HPO_3)_2$.

Fig. S1. Experimental and calculated powder X-ray diffraction patterns of $Pb_2(HPO_3)_2$ (**a**) and $Pb_2(HPO_3)(NO_3)_2$ (**b**).

Fig. S2. IR spectra of $Pb_2(HPO_3)_2$ (**a**) and $Pb_2(HPO_3)(NO_3)_2$ (**b**).

Fig. S3. View of structure of compound $Pb_2(HPO_3)(NO_3)_2$ down the *c* axis.

Fig. S4. UV-vis-NIR absorption spectra of $Pb_2(HPO_3)_2$ and $Pb_2(HPO_3)(NO_3)_2$.

Fig. S5. The band structure of $Pb_2(HPO_3)(NO_3)_2$.

Fig. S6 Total and partial density of states of $Pb_2(HPO_3)(NO_3)_2$.

Table S1.

Atom	x	y	z	U(eq)
Pb(1)	17256(1)	7796(1)	14911(1)	20(1)
Pb(2)	20000	5369(1)	13148(1)	19(1)
Pb(3)	15000	5794(1)	13156(2)	36(1)
P(1)	15000	7046(5)	17277(9)	10(1)
P(2)	17431(4)	5310(3)	15827(7)	15(1)
P(3)	15000	7972(4)	11911(9)	12(1)
O(1)	16150(13)	7528(11)	17867(19)	24(3)
O(4)	18645(11)	4816(11)	15754(19)	27(4)
O(5)	17349(16)	6114(12)	14600(30)	49(6)
O(7)	15000	8739(12)	13140(30)	29(4)
O(6)	16116(16)	7351(13)	12060(20)	33(4)
O(3)	16391(12)	4638(12)	15630(30)	43(5)
O(2)	15000	6982(17)	15450(30)	39(6)

Table S2.

Pb(1)-O(5)	2.422(17)	Pb(3)-O(6)	2.70(2)
Pb(1)-O(1)#1	2.478(15)	Pb(3)-O(6)#10	2.70(2)
Pb(1)-O(6)#2	2.531(17)	Pb(3)-O(5)#10	2.91(2)
Pb(1)-O(6)	2.720(19)	Pb(3)-O(5)	2.91(2)
Pb(1)-O(1)	2.731(16)	Pb(3)-O(3)#10	3.033(18)
Pb(1)-O(2)	2.805(12)	Pb(3)-O(3)	3.033(18)
Pb(1)-O(3)#3	3.092(18)	P(1)-O(2)	1.49(2)
Pb(1)-O(4)#3	3.136(16)	P(1)-O(1)	1.532(15)
Pb(2)-O(7)#4	2.333(17)	P(1)-O(1)#10	1.532(15)
Pb(2)-O(4)#5	2.480(15)	P(2)-O(3)	1.514(15)
Pb(2)-O(4)#6	2.480(15)	P(2)-O(5)	1.53(2)
Pb(2)-O(4)	2.721(14)	P(2)-O(4)	1.527(13)
Pb(2)-O(4)#7	2.721(14)	P(3)-O(7)	1.49(2)
Pb(3)-O(2)	2.53(2)	P(3)-O(6)#10	1.532(16)
Pb(3)-O(3)#9	2.648(18)	P(3)-O(6)	1.532(16)
Pb(3)-O(3)#5	2.648(17)		
O(1)-Pb(1)#2	2.478(15)	O(7)#4-Pb(2)-O(4)#5	83.8(7)

O(4)-Pb(2)#8	2.480(15)	O(7)#4-Pb(2)-O(4)#6	83.8(7)
O(4)-Pb(1)#11	3.136(16)	O(4)#5-Pb(2)-O(4)#6	75.0(6)
O(7)-Pb(2)#12	2.333(17)	O(7)#4-Pb(2)-O(4)	73.2(7)
O(6)-Pb(1)#1	2.531(17)	O(4)#5-Pb(2)-O(4)	104.2(4)
O(3)-Pb(3)#13	2.648(17)	O(4)#6-Pb(2)-O(4)	156.85(9)
O(3)-Pb(1)#11	3.092(18)	O(7)#4-Pb(2)-O(4)#7	73.2(7)
O(2)-Pb(1)#10	2.805(11)	O(2)-Pb(3)-O(3)#9	137.0(5)
O(5)-Pb(1)-O(1)#1	73.3(6)	O(2)-Pb(3)-O(3)#5	137.0(5)
O(5)-Pb(1)-O(6)#2	87.7(7)	O(3)#9-Pb(3)-O(3)#5	71.6(7)
O(1)#1-Pb(1)-O(6)#2	86.3(4)	O(2)-Pb(3)-O(6)	71.9(7)
O(5)-Pb(1)-O(6)	72.4(7)	O(3)#9-Pb(3)-O(6)	101.9(6)
O(1)#1-Pb(1)-O(6)	73.6(5)	O(3)#5-Pb(3)-O(6)	70.6(5)
O(6)#2-Pb(1)-O(6)	154.9(3)	O(2)-Pb(3)-O(6)#10	71.9(7)
O(5)-Pb(1)-O(1)	88.4(6)	O(3)#9-Pb(3)-O(6)#10	70.6(5)
O(1)#1-Pb(1)-O(1)	152.8(3)	O(3)#5-Pb(3)-O(6)#10	101.9(6)
O(6)#2-Pb(1)-O(1)	72.6(5)	O(6)-Pb(3)-O(6)#10	54.8(7)
O(3)#9-Pb(3)-O(5)#10	79.9(6)	O(2)-Pb(3)-O(5)#10	66.1(4)

Symmetry transformations used to generate equivalent atoms: #1 -x-3/2, -y+1/2, z+1/2; #2 -x-3/2, -y+1/2, z-1/2; #3 -x-3/2, y-1/2, z; #4 x-1/2, y+1/2, z; #5 x, -y+1, z+1/2; #6 -x-2, -y+1, z+1/2; #7 -x-2, y,

z; #8 -x-2, -y+1, z-1/2; #9 -x-1, -y+1, z+1/2; #10 -x-1, y, z; #11 -x-3/2, y+1/2, z; #12 x+1/2, y-1/2, z; #13 -x-1, -y+1, z-1/2.

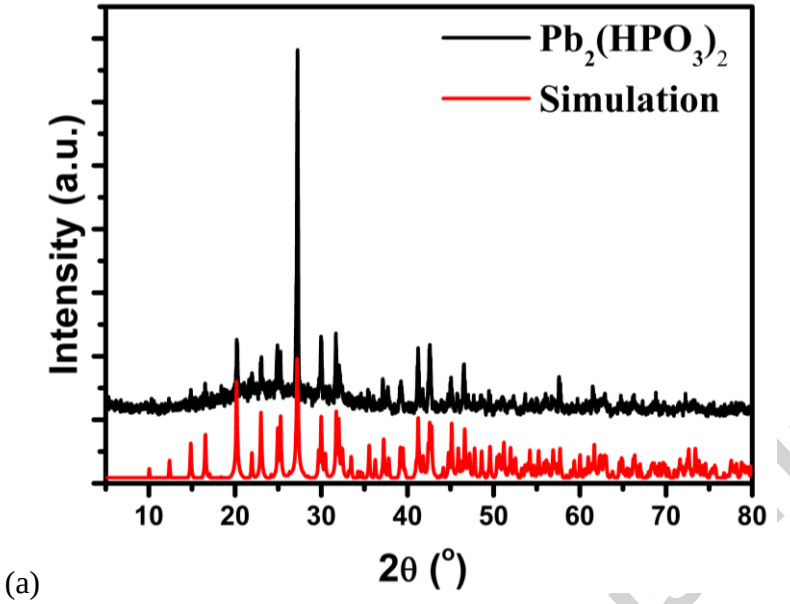

(a)

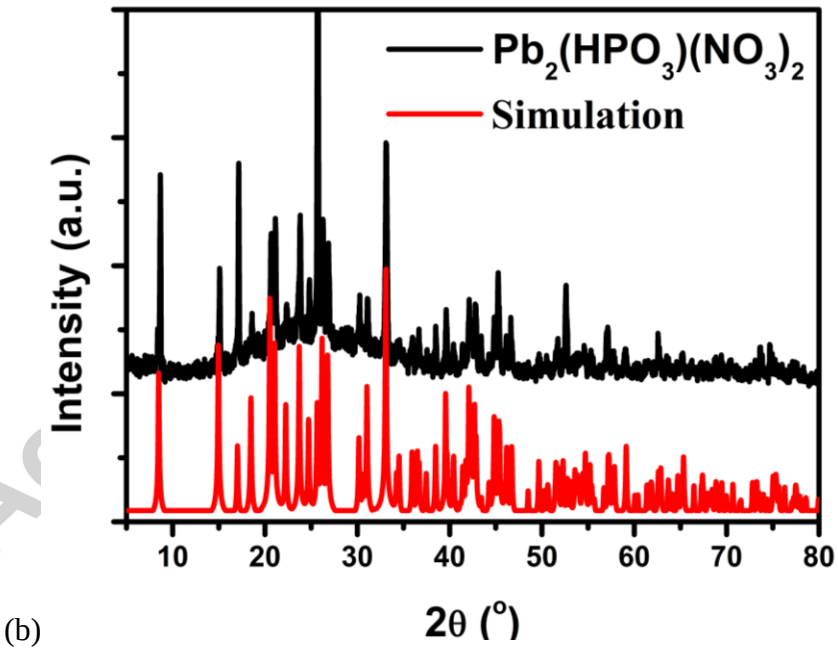

(b)

Fig. S1.

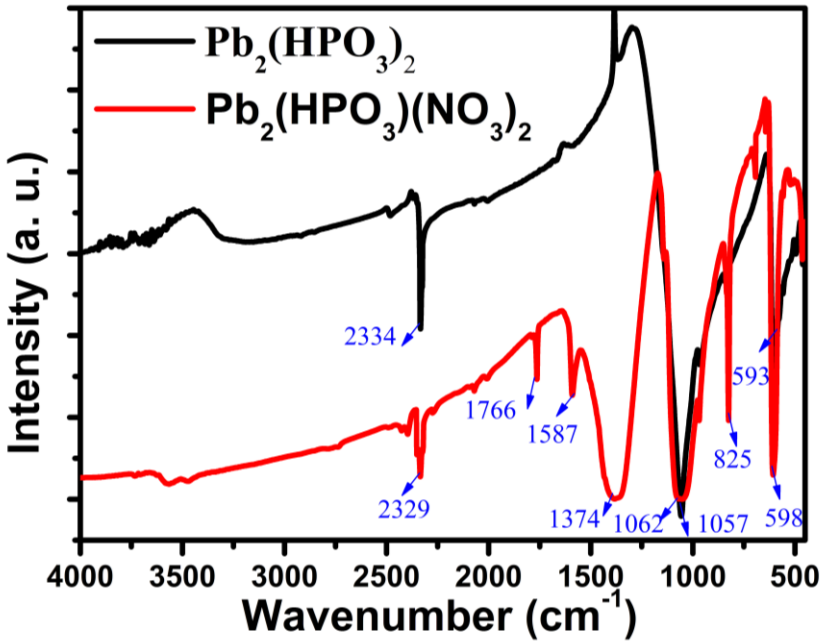
Pb2(HPO3)2
Pb2(HPO3)(NO3)2
Intensity (a. u.)
2334
1766
1587
593
825
2329
1374
1062
1057
598
4000
3500
3000
2500
2000
1500
1000
500
Wavenumber (cm-1)

Fig. S2.

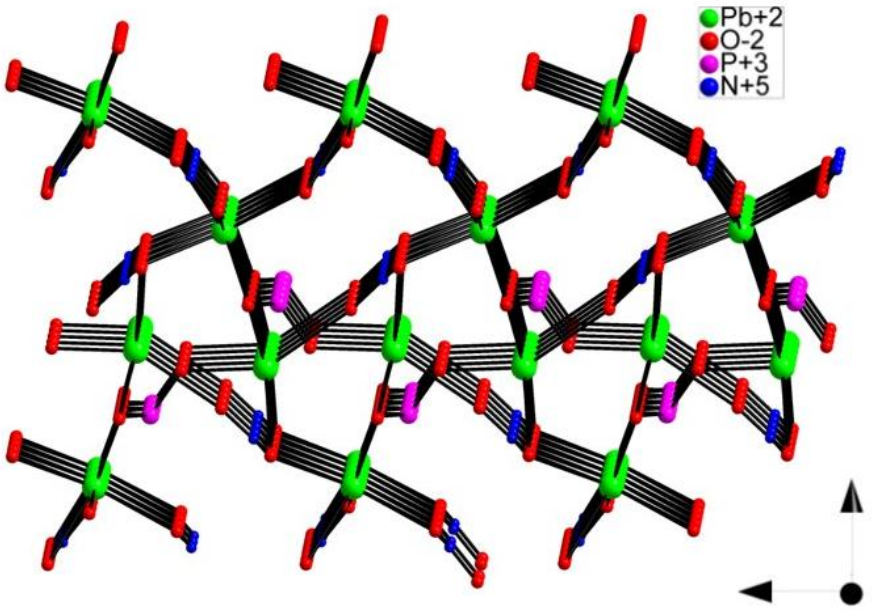
Pb+2
O-2
P+3
N+5

Fig. S3.

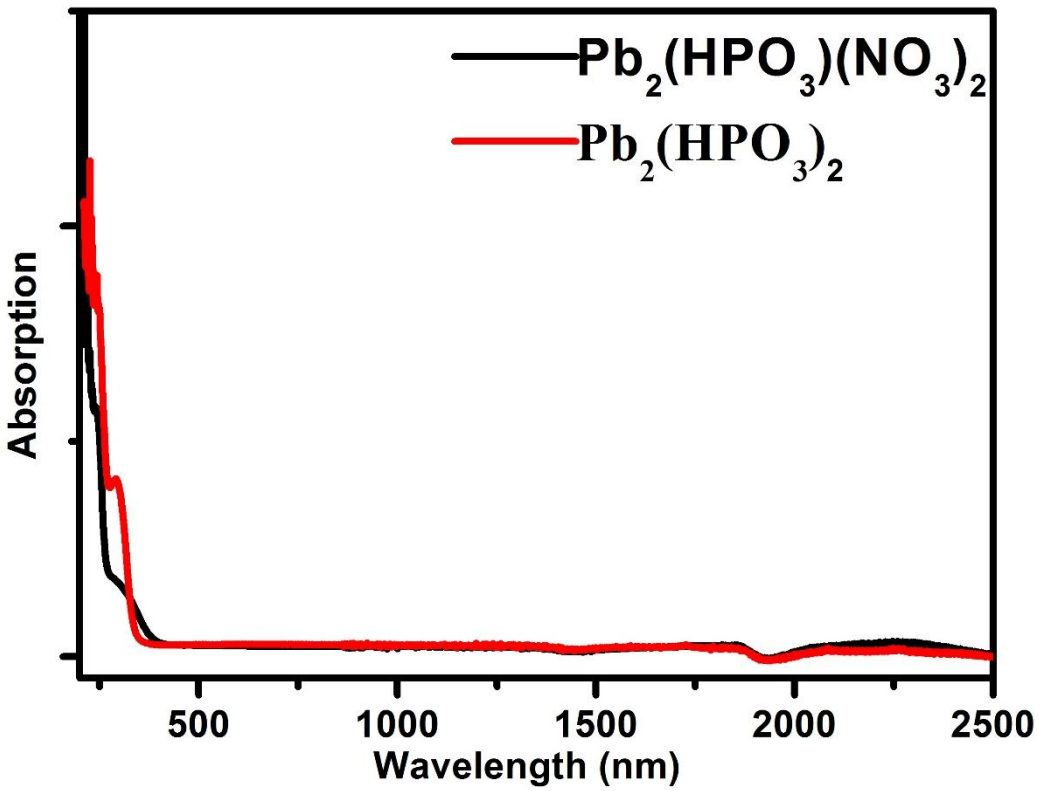
Pb2(HPO3)(NO3)2
Pb2(HPO3)2
Absorption
500
1000
1500
2000
2500
Wavelength (nm)

Fig. S4.

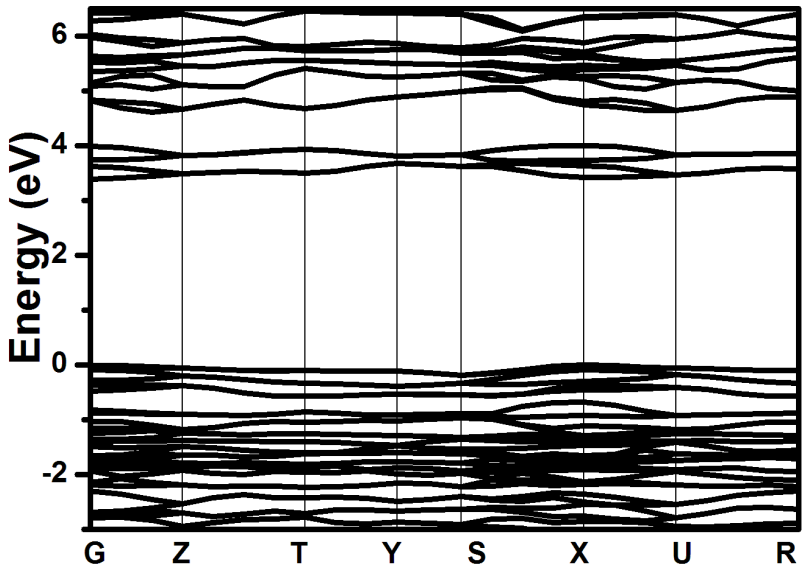
6
4
2
0
-2
Energy (eV)
G
Z
T
Y
S
X
U
R

Fig. S5.

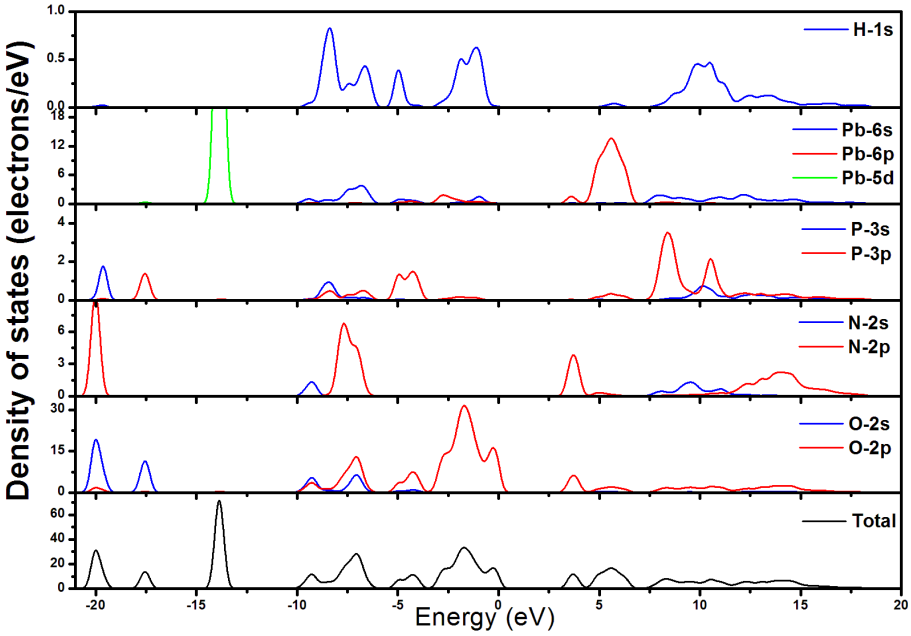

Fig. S6.